*fractal and fractional*

MDPI

*Article*

# Multifractal Structures and the Energy-Economic Efficiency of Chinese Cities: Using a Classification-Based Multifractal Method

**Jiaxin Wang [1,2,*], Bin Meng [1,2] and Feng Lu [3,4]**

[1] College of Applied Arts and Sciences, Beijing Union University, Beijing 100191, China; mengbin@buu.edu.cn
[2] Laboratory of Urban Cultural Sensing & Computing, Beijing Union University, Beijing 100191, China
[3] State Key Laboratory of Resources and Environmental Information System, Institute of Geographic Sciences and Natural Resources Research, Chinese Academy of Sciences, Beijing 100101, China; luf@lreis.ac.cn
[4] University of Chinese Academy of Sciences, Beijing 100049, China
* Correspondence: wangjx_buu@163.com

**Abstract:** Improper urban spatial structure can lead to problems such as traffic congestion, long commuting times, and diseconomies of scale. Evaluating the efficiency of urban spatial structure is an important means to enhance the sustainable development of cities. The fractal method has been widely used in the identification and efficiency evaluation of urban spatial structure due to its sufficient characterization of urban complexity. However, the identification of urban fractal structures has expanded from monofractal structures to multifractal structures, while the efficiency evaluation of urban fractal structures remains limited to the single-dimensional efficiency evaluations of single fractals, seriously affecting the reliability of urban fractal structure evaluation. Therefore, this study identifies and evaluates urban spatial structure within the unified framework of multifractal analysis. Specifically, a classification-based multifractal method is introduced to identify the multifractal structure of 290 cities in China. An iterative application of the geographic detector method is used to evaluate the comprehensive energy-economic efficiency of urban multifractal structures. The results indicate that the 290 Chinese cities include 6 typical multifractal structures. The explanatory power of these six typical multifractal structures for urban energy-economic efficiency is 16.27%. The advantageous multifractal structures of cities that achieve higher energy-economic efficiency rates satisfy a cubic polynomial form. By comparing them with the advantageous multifractal structures, the main problems affecting the efficiency of urban multifractal structures in the other five types of cities are shown to include overly strong or weak concentration capacity of high-level centers, weak hierarchical structures among centers, and the spreading of low-level centers.

**Keywords:** multifractal structure; energy-economic efficiency; nighttime light; Chinese cities



Academic Editor: Yanguang Chen

Received: 19 December 2024
Revised: 26 January 2025
Accepted: 30 January 2025
Published: 3 February 2025

**Citation:** Wang, J.; Meng, B.; Lu, F. Multifractal Structures and the Energy-Economic Efficiency of Chinese Cities: Using a Classification-Based Multifractal Method. *Fractal Fract.* **2025**, *9*, 96. https://doi.org/10.3390/fractalfract9020096



## 1. Introduction

Currently, about half of the global population, approximately 3.5 billion people, live in cities. By 2030, nearly 60% of the world's population, around 5 billion people, will reside in urban areas. As the second most populous country in the world, China's urbanization rate reached 66% in 2023, with over 900 million people living in cities. These populations engage in a range of socio-economic activities in cities, consuming enormous amounts of energy. In 2023, the global energy distribution included oil (29.61%), coal (25.07%), natural gas (22.03%), biomass (6.21%), nuclear (3.75%), hydro (6.32%), wind (3.07%), solar (1.93%), biofuels (0.66%), and other alternative energy sources (1.35%). This energy usage led to emissions of around 37.55 GTCO2, representing a 1.1% rise from 2022 and being roughly

60% higher than the $CO_2$ emissions that were recorded in 1990. The spatial structure of a city affects the efficiency of socio-economic activities. An improper spatial structure can lead to traffic congestion, long commuting times, and economies of scale, thereby increasing the energy consumption, reducing the economic output, and impacting urban sustainable development [1,2]. Therefore, assessing the energy-economic efficiency of urban spatial structures is an important means to enhance the level of urban sustainable development.

Accurately quantifying the urban spatial structure is a prerequisite for conducting energy-economic efficiency assessments of the urban spatial structure. Existing research has depicted urban spatial structure from perspectives such as the spatial concentration of urban elements [3,4], the spatial centralization of urban elements towards the CBD [5–7], and the fractal structure of the urban hierarchy [8–11]. In comparison, fractal structures exhibit the self-similarity of urban hierarchical systems, clearly depicting the spatial complexity and livingness of cities [12–14]. A large body of research also emphasizes the importance of urban fractal structures for better understanding the livingness of urban spatial structures, urban spatial order, and the efficiency of urban metabolism [15–17]. Existing methods for characterizing urban fractal structures include monofractal methods and multifractal methods. Among them, the monofractal method belongs to global models and uses global parameters to characterize urban self-similarity, including geometric fractal dimension, network fractal dimension, flow fractal dimension, the Ht index, etc. [18–22]. The multifractal method belongs to local models, considering the different growth probabilities of urban elements in various locations, thereby potentially presenting heterogeneous self-similar structures [23–25]. Traditional moment-based multifractal methods can fully capture the fractal heterogeneity of urban space. However, it lacks an explicit mapping relationship with geographic space, making the hierarchical relationship between the multifractal structure and the urban center unclear. To enhance the spatial display and interpretability of the multifractal structure, Tan et al. [26] proposed modeling the density relationship between urban plots and surrounding areas using the slope coefficient from a local perspective and then identifying typical spatial organization patterns through cluster analysis. Wang et al. [27] identified the urban hierarchy system by classifying urban elements according to density and then hierarchically identifying the multifractal structure of urban elements, referred to as the classification-based multifractal method. In contrast, the classification-based multifractal method directly depicts the multifractal structure of the urban hierarchy system, with clear spatial meanings of the multifractal parameters.

Evaluating the efficiency of existing urban fractal structures primarily focuses on assessing the efficiency of monofractal structures. The main evaluation methods include the allometric growth method and statistical analysis. The allometric growth method is used to assess the relationship between urban monofractal structures and natural or socio-economic indicators. For example, Lu and Tang [28] measured urban accessibility using the fractal dimension of the transportation network and evaluated the allometric growth relationship between fractal dimensions and the urban population. Lan et al. [29] established the allometric growth relationships between the fractal dimension of Hong Kong's road network structure and socio-economic indicators such as the urban population, GDP, and $CO_2$ emissions. They found an inverse allometric growth relationship between the structural fractal dimension of the road network and the area of cultivated and agricultural land. Lan et al. [30] measured the allometric growth relationships between the fractal dimension of urban subway networks and the urban economy, population, and environment. The statistical analysis method is often used to evaluate the impact of monofractal land use structures on the urban environment and ecology. For example, Xu et al. [31] used the perimeter–radius fractal dimension to measure the adjacency and landscape fragmentation among different land use patches. They applied the geographical

detector method to analyze its impact on regional carbon sequestration. The results showed that as the spatial structure of land use transitioned from complex to simple, the influence of landscape characteristics on regional carbon sequestration gradually decreased. Lu and Liu [18] used a boundary dimension to characterize the complexity of urban land use boundaries as one of the indicators describing the urban morphology. They established a geographically weighted regression model to evaluate the impact of the urban morphology on air quality, revealing that fractal dimensions had no significant impact on air quality. In summary, few studies have conducted efficiency evaluations of urban multifractal structures. Moreover, existing evaluations of urban fractal structures primarily focus on single dimensions such as the economy, energy, or the environment, lacking a comprehensive multidimensional efficiency assessment.

Therefore, this study introduces a classification-based multifractal method to characterize the multifractal structures of 290 cities in China. From the input–output perspective, energy-economic composite indicators are constructed to evaluate the efficiency of urban multifractal structures. The geographical detector method is iteratively applied to assess the comprehensive energy-economic efficiency of urban multifractal structures, identifying advantageous multifractal structures with higher energy-economic efficiency. Furthermore, spatial structure issues affecting the overall urban energy-economic efficiency are diagnosed.

## 2. Materials and Methods

### *2.1. Study Area and Data*

There are 293 prefecture-level cities in China, and based on data availability, this study evaluates the urban multifractal structure and energy-economic efficiency of 290 prefecture-level cities, which are close to the entire sample of cities. The concept of prefecture-level cities is an administrative region, and urban socio-economic activities mainly occur in the physical area of these cities. Therefore, the study area is the physical area of 290 prefecture-level cities in China. The key to the identification of urban physical areas is the threshold determination of urban and non-urban areas. Cao et al. [32] proposed a percolation-based method to optimize urban and non-urban thresholds by considering the critical nature of urban systems. Taking nighttime lighting (NTL) as an example, when extracting the urban area, if the threshold of urban and non-urban division is less than the 3DN value, a giant cluster quickly forms. Therefore, the 3DN value is the optimal threshold. Based on Cao's results, areas with an NTL brightness greater than 3 and a cluster size greater than 20 $km^2$ were identified as urban physical areas.

The NTL brightness data were used to study the multifractal structures of Chinese cities. The NTL brightness records the composite information under the interaction of urban socio-economic activities, which is an ideal data source for effectively portraying urban spatial structures [33], and Li et al. [34] also pointed out that nighttime light reflects the spatial distribution of the migrant population, which is more reflective of the real urban spatial structure. Some studies have also shown that urban nighttime lighting represents fractal and multifractal spatial structures [15,35]. Chen et al. [36] developed an auto-encoder model including convolutional neural networks to integrate Defense Meteorological Satellite Program-Operational LinescanSystem (DMSP-OLS) NTL and National Polar-orbiting Partnership-Visible infrared Imaging Radiometer (NPP-VIIRS) NTL data and generated an extended time series of global annual NPP-VIIRS-like NTL data (https://doi.org/10.7910/DVN/YGIVCD). In this study, the multifractal structures of Chinese cities were modeled using NPP-VIIRS-like NTL data for 2019, which was chosen to avoid the impact of the COVID-19 pandemic.

Regarding the energy-economic indicators that were used to optimize the urban spatial structure, a total of three indicators were selected: GDP, GDP per capita, and GDP per unit of electricity consumption (Figure 1). Here, GDP represents the size of the economy, GDP per capita represents the living standard, and GDP per unit of electricity consumption represents the energy utilization efficiency of economic development. The basic data that were needed to generate the three indicators include the GDP, population, and electricity consumption of the urban physical area. The GDP data were generated from the grid GDP data from the Resource and Environment Science and Data Center (https://www.resdc.cn/, accessed on 25 January 2025) [37]; the population data were generated from the Landscan grid population data, released by Oak Ridge National Laboratory (https://landscan.ornl.gov/, accessed on 25 January 2025) [38]; and the electricity consumption data were estimated from Wang et al.'s [35] model.

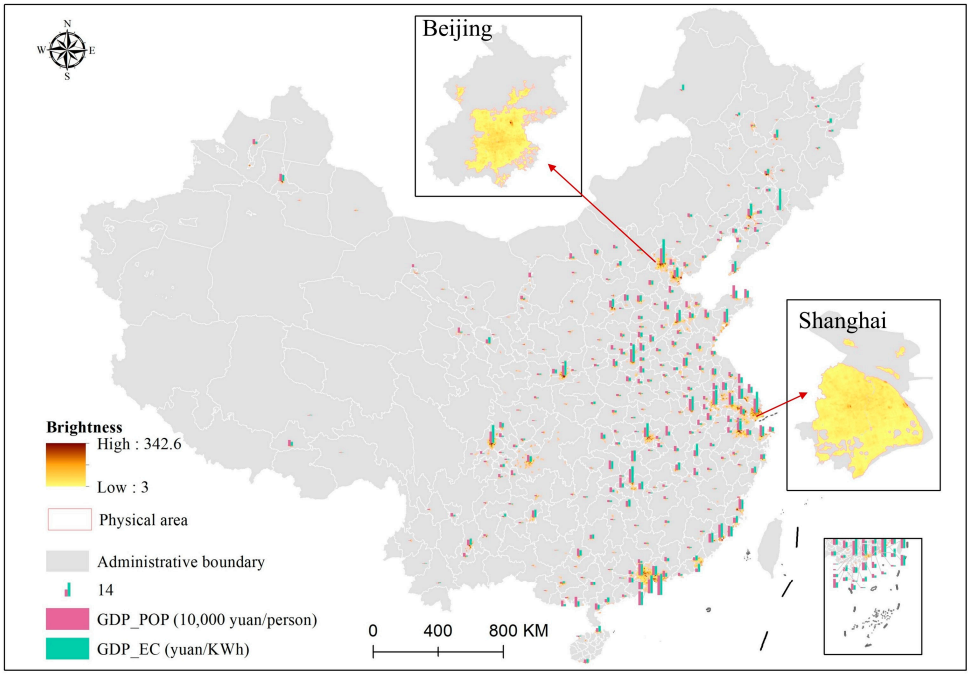


**Figure 1.** Study area and data.

## 2.2. Methods

Figure 2 shows the research technology roadmap of this study. The identification and optimization of urban multifractal structures mainly includes three modules: a quantitative representation of the urban multifractal structure, typical characteristics, and a performance evaluation. The methods used in each module are described in the following.

(1) The CMFA method: identifying urban multifractal structures

This study uses the CMFA method to quantify the multifractal structure of urban nighttime lights. Traditional multifractal analysis methods implicitly highlight different density zones by changing the statistical moments of urban elements. Therefore, although the multifractal spectrum portrays the heterogeneous scaling structure of the urban local area, the mapping relationship between the local geographical space and the scaling characteristics is unclear; that is, the points on the multifractal spectrum lack geographic information. When the multifractal spectrum indicates the existence of anomalies in the multifractal structure of a city, the lack of geographic information makes it impossible to target the areas with anomalous structures and thus cannot directly guide the optimization of the urban spatial structure. The CMFA method remedies this deficiency: this is achieved by dividing the urban area into several subregions with different density classes and then

constructing fractal indicators to portray the density–form characteristics of each subregion, specifically the singularity exponent ($\alpha_{s_i}$) reflecting the agglomeration degree of different density zones and the fractal dimension ($f(\alpha_{s_i})$) reflecting the concentration degree of different density zones:

$$\overline{\mu}_{s_i}(\varepsilon) = \frac{\sum_x \mu_{x,s_i}(\varepsilon)}{N(\alpha_{s_i},\varepsilon)} \sim \varepsilon^{\alpha_{s_i}}, \quad (1)$$

$$N(\alpha_{s_i},\varepsilon) \sim \varepsilon^{-f(\alpha_{s_i})}, \quad (2)$$

Here, $s_i$ is the subregion with a different socio-economic density. $\overline{\mu}_{s_i}(\varepsilon)$ is the average density of subregion $s_i$ at scale $\varepsilon$. $\mu_{x,s_i}(\varepsilon)$ is the density at location $x$ within subregion $s_i$ at scale $\varepsilon$. $N(\alpha_{s_i},\varepsilon)$ is the space that is occupied by subregion $s_i$ at scale $\varepsilon$. $\alpha_{s_i}$ is the singularity exponent, which describes the power-law relationship between the average density of subregion $s_i$ and the observed scale $\varepsilon$, uncovering the density agglomeration degree. $f(\alpha_{s_i})$ is the fractal dimension, which portrays the power-law relationship between the space that is occupied by subregion $s_i$ and the observed scale $\varepsilon$, representing the space-filling capacity. The singularity exponent and fractal dimension reflect the self-similarity of the density and form in different subregions of the city. The pairs of singularity exponents and fractal dimensions in different subregions are called the multifractal spectrum, representing the urban multifractal structure.

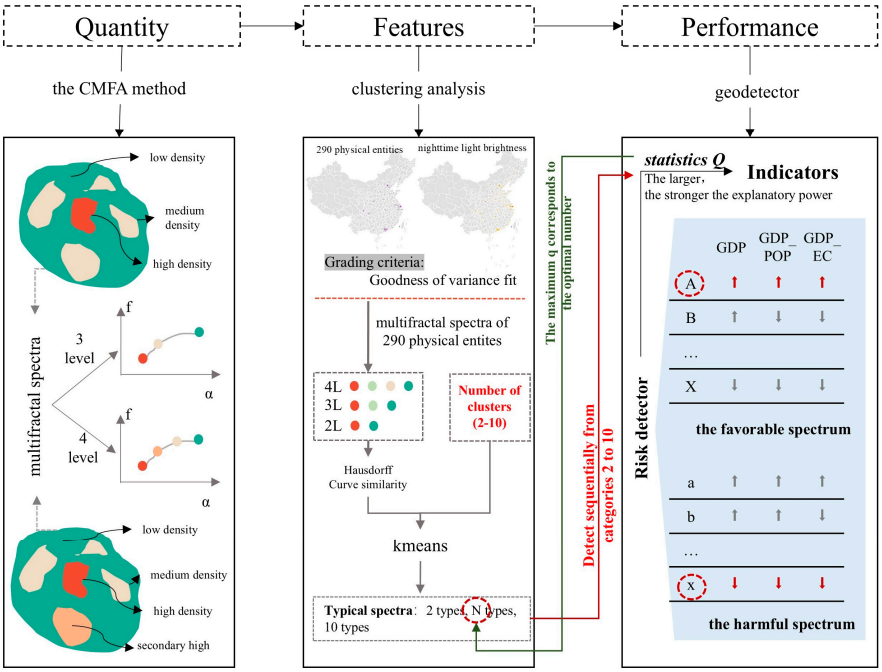


**Figure 2.** The technology roadmap for this study.

Figure 3 simulates several socio-economic densities of urban spatial distributions to understand the relationship between the multifractal spectrum, taking into account the geographic mapping and the urban density–form distribution. It is assumed that the socio-economic density within the simulated city has a 3-level structure, which are high-density, medium-density, and low-density zones. Figure 3A,B have the same socio-economic densities, but the spatial distribution patterns of density are different: for the same density zone, the former is distributed in a more decentralized manner, and the latter is distributed in a more centralized manner. Figure 3B,C have the same spatial distribution patterns for different levels of density zones, but the socio-economic densities of the high-density zones are different, and the latter is denser than the former.

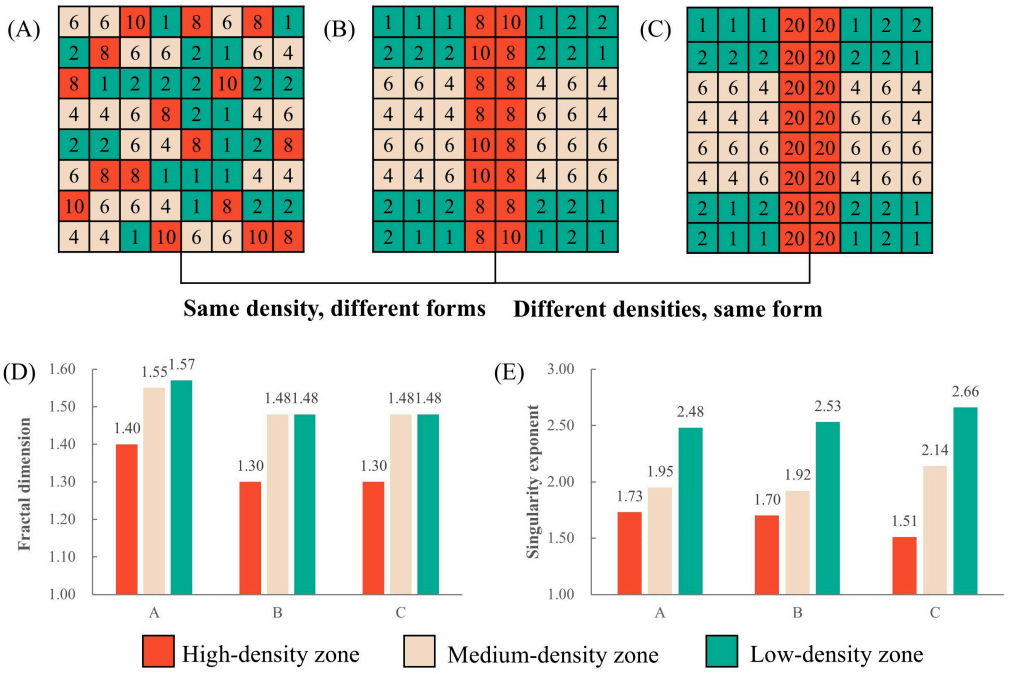


**Figure 3.** Three simulated maps of urban socio-economic density distributions and comparisons of their multifractal spectra. (**A**,**B**) have the same densities and different forms. (**B**,**C**) have the same forms and different densities. (**D**) The fractal dimensions of the three socio-economic density distributions. (**E**) The singularity exponents of the three socio-economic density distributions.

Figure 3D compares the fractal dimensions of the three socio-economic density distributions. Since the distribution patterns of Figure 3B,C are the same, the fractal dimensions of the different density zones of both are also the same, indicating the same centralization degree of different density zones. The spatial distribution of the different density zones in Figure 3A is more decentralized, and different density zones occupy more space at different scales than in Figure 3B, so their fractal dimension is also larger.

Figure 3E compares the singularity exponents of the three-level socio-economic density distributions, although the socio-economic densities of Figure 3A,B are the same, but the centralized distribution of form has a pulling effect on the average density gradient between levels, so the singularity exponents of Figure 3A,B are closer but not exactly the same, and the singularity of the former is slightly greater than that of the latter. The high-density zones of Figure 3C have higher socio-economic densities than that of Figure 3B. The density gradient of Figure 3C between different levels is greater, so their singularity exponents are smaller for high-density zones and greater for low-density zones. This indicates that the socio-economic agglomeration of high-density zones in Figure 3C is greater than that in Figure 3B.

(2) Geodetector: Optimizing the urban spatial structures

The geodetector method was used to measure the correlation between the urban spatial structures and energy-economic performance (GDP, GDP per capita, and GDP per unit of electricity consumption). The basic idea of a geodetector is to assume that the study area is divided into L strata, and if the sum of the variances of the variables in each stratum is less than the total regional variance, it indicates that there is spatial heterogeneity in the variables, meaning that the variables are significantly different between strata [39].

Here, in order to determine the optimized urban spatial structure, the 290 urban spatial structures were classified into 2 to 10 classes using the *k*means algorithm. A geodetector was iteratively used to detect the correlation between urban spatial structures and energy-economic indicators.

Specifically, the factor detector was used to detect the spatial heterogeneity of the variable Y (the energy-economic indicator) on the classification variable $x$ (the clustering of the multifractal spectra).

$$q = 1 - \frac{\sum_{h=1}^{L} N_h \sigma_h^2}{N\sigma^2} \tag{3}$$

where $h$ = 1, …, and $L$ is the stratum of variable $x$; $N_h$ and $N$ are the number of cities belonging to the stratum $h$ and the total quantity; and $\sigma_h^2$ and $\sigma^2$ are the variance of variable Y belonging to the stratum $h$ and the total quantity. $q$ is within the range of [0–1]. The larger the value of $q$ is, the more significant the spatial heterogeneity is.

The risk detector was used to determine whether the mean values of the attributes were significantly different between strata and was tested with the t-statistic.

$$t_{\overline{y}_{h-1} - \overline{y}_{h-2}} = \frac{\overline{Y}_{h=1} - \overline{Y}_{h=2}}{\left[ \frac{\mathrm{Var}\left(\overline{Y}_{h=1}\right)}{n_{h=1}} + \frac{\mathrm{Var}\left(\overline{Y}_{h=2}\right)}{n_{h=2}} \right]^{1/2}} \tag{4}$$

where $\overline{Y}_h$ represents the mean value of attributes (GDP, GDP per capita, or GDP per unit of electricity consumption) within stratum $h$; $n_h$ is the number of cities belonging to stratum $h$; and Var represents the variance.

(3) Uncertainty of the results

The major sources of uncertainty are related to the most important parameters in identifying and classifying the multifractal structures of cities [40]:

(a) The GVF threshold

The key to the identification of multifractal spectra is to determine the hierarchical number of urban areas. In order to ensure that different cities are classified equally, a uniform GVF is used to determine the hierarchical number of cities. The GVF threshold is a source of uncertainty when identifying the multifractal structure of cities. This study used the following conditions to evaluate the impact of different GVF thresholds on the classification results in order to determine an appropriate threshold: if the classified number was increased and the GVF did not change much, meaning that the improvement degree of the classification effect was limited, then the increase in the classified number should be stopped. The improvement degree (ID) is defined as follows:

$$\mathrm{ID} = \frac{(GVF_{i+1} - GVF_i)}{GVF_i} \times 100\% \tag{5}$$

where $i$ represents the classified number.

(b) The number of classes

The number of classes is a source of uncertainty in identifying typical multifractal structures, which affects their energy-economic efficiency evaluation. This study evaluated the energy-economic efficiency of typical multifractal structures from 2 to 10 classes and determined the appropriate number of classes.

## 3. Results and Discussions

### *3.1. Multifractal Structures of 290 Cities*

Figure 4 shows the scatter plot of the GVF and ID in 290 urban physical areas, which can be fitted with a cubic polynomial curve ($R^2$ = 0.89). When the GVF is small, increasing the GVF can improve the ID; when the GVF increases to 0.8, which is the first turning point of the cubic polynomial curve, and continues to increase, the overall improvement in the ID is also larger, but with a decreasing trend; after the GVF increases to about 0.88, which is the second turning point of the cubic polynomial curve, and continues to increase, the

overall improvement of the ID is smaller. Therefore, the GVF threshold for the hierarchical number of urban areas was set to 0.88.

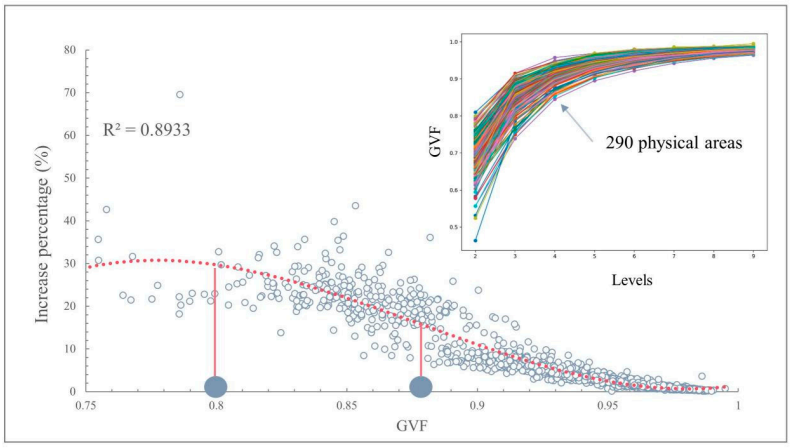


**Figure 4.** The threshold of GVF.

The results indicate that the number of hierarchical levels in the 290 urban physical areas includes two levels (41 areas, 14.14%), three levels (232 areas, 80%), and four levels (17 areas, 5.86%). There is a significant relationship between the number of levels and the size of the urban physical areas (Figure 5c): for cities with two levels, the height of the box plot is low, indicating that the size of the urban physical areas within this category is generally low, with an average area of 100.54 km$^2$; for cities with three levels, the average size of the physical areas is 330.75 km$^2$, but there are a number of outlying points comprising 20 cities; for cities with four levels, the height of the box plot is greater, indicating that the size of the urban physical areas within this category varies considerably, but the overall size is larger, with an average area of up to 1833.68 km$^2$.

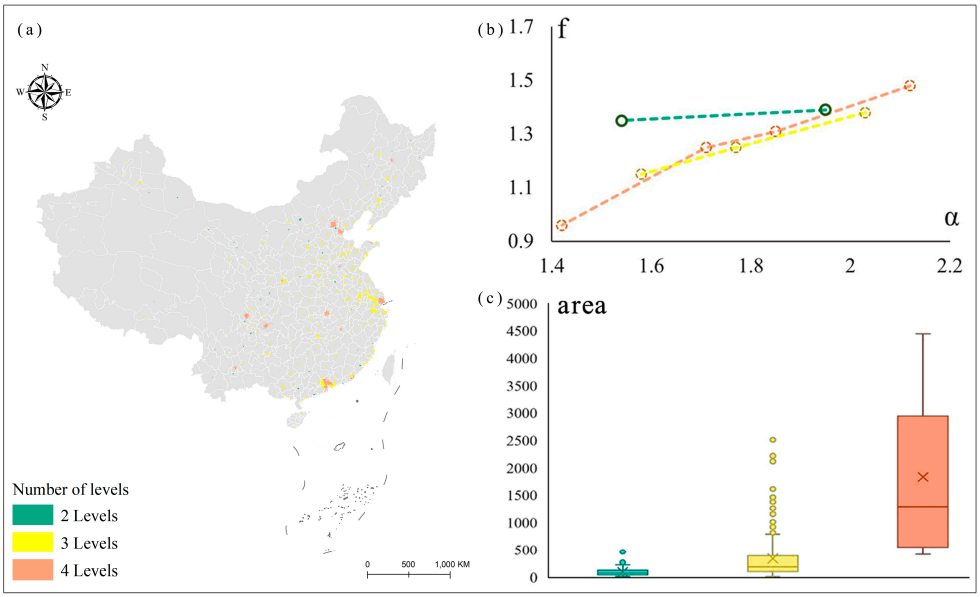


**Figure 5.** The features of the multifractal spectra of the 290 urban physical areas. (**a**) The spatial distribution of urban levels. (**b**) The average multifractal spectra of cities with different numbers of levels. (**c**) The area box plot for cities with different levels.

Figure 5b shows the average multifractal spectra of cities with different numbers of levels, where the average multifractal spectra of urban polycentric spatial organizations with four levels are distributed between (1.42, 0.96) and (2.12, 1.48); the average multifractal

spectra of urban polycentric spatial organizations with three levels are distributed between (2.03, 1.38) and (1.58, 1.15); and the average multifractal spectra of urban polycentric spatial organizations with two levels are distributed between (1.95, 1.39) and (1.54, 1.35). On average, the higher the number of hierarchical levels is, the greater the heterogeneity of the density and morphological distribution are.

### *3.2. The Typical Multifractal Structures of the 290 Cities*

The bidirectional Hausdorff distance was chosen to calculate the similarity of the multifractal spectra of the 290 cities. Then, the *k*means algorithm was used to classify the 290 multifractal spectra into several typical classes to reflect the typical multifractal structures. Table 1 shows the *q* statistic values of GDP, GDP per capita, and GDP per unit of electricity consumption under different classifications of the multifractal spectra.

**Table 1.** *q* statistics of three indicators under 2–10 classes of multifractal spectra.

| **For GDP** | | | | | |
|---|---|---|---|---|---|
| | **2 Classes** | **3 Classes** | **4 Classes** | **5 Classes** | **6 Classes** |
| *q* statistic | 4.22% | 8.10% | 8.08% | 7.62% | 10.51% |
| *p* value | 0.000 | 0.000 | 0.000 | 0.000 | 0.000 |
| | **7 Classes** | **8 Classes** | **9 Classes** | **10 Classes** | |
| *q* statistic | 10.02% | 10.02% | 12.52% | 13.62% | |
| *p* value | 0.000 | 0.000 | 0.000 | 0.000 | |
| **For GDP Per Capita** | | | | | |
| | **2 Classes** | **3 Classes** | **4 Classes** | **5 Classes** | **6 Classes** |
| *q* statistic | 5.70% | 14.75% | 18.16% | 17.34% | 23.51% |
| *p* value | 0.000 | 0.000 | 0.000 | 0.000 | 0.000 |
| | **7 Classes** | **8 Classes** | **9 Classes** | **10 Classes** | |
| *q* statistic | 21.00% | 21.28% | 24.05% | 21.11% | |
| *p* value | 0.000 | 0.000 | 0.000 | 0.000 | |
| **For GDP Per Unit of Electricity Consumption** | | | | | |
| | **2 Classes** | **3 Classes** | **4 Classes** | **5 Classes** | **6 Classes** |
| *q* statistic | 4.08% | 10.87% | 12.93% | 11.29% | 17.15% |
| *p* value | 0.000 | 0.000 | 0.000 | 0.000 | 0.000 |
| | **7 Classes** | **8 Classes** | **9 Classes** | **10 Classes** | |
| *q* statistic | 15.38% | 15.46% | 17.02% | 17.17% | |
| *p* value | 0.000 | 0.000 | 0.000 | 0.000 | |

Regarding the spatial heterogeneity of GDP under different classifications of multifractal spectra, the *q* values were statistically significant at all clustering numbers. In terms of the magnitude of the *q* value, the explanatory power of the spectral features under two classes was the weakest for a GDP of 4.22%; the explanatory power of the spectral features under three, four, and five classes was close to about 8%; the explanatory power of the spectral features under six, seven, and eight classes was close to about 10%; and the explanatory power of the spectral features under nine and ten classes was close to and the largest at about 13%. The explanatory power did not increase much from six to nine classes. Therefore, six was the best-classified number for the GDP effect, with an explanatory power of 10.51%.

Regarding the spatial heterogeneity of GDP per capita under different classifications of the multifractal spectra, the *q* values were also statistically significant at all clustering numbers. The *q* value was smallest under two classes at 5.70%; the *q* value continued to increase from three classes to six classes, reaching 23.51% for six classes and changing slowly beyond six classes. Therefore, six was also the best-classified number for the GDP per capita effect, with an explanatory power of 23.51%.

Regarding the spatial heterogeneity of GDP per unit of electricity consumption under different classifications of the multifractal spectra, the $q$ values were also statistically significant at all clustering numbers. The $q$ value increased gradually as the clustering number increased until six classes. Therefore, six was also the best-classified number for the GDP per unit of electricity consumption effect, with an explanatory power of 17.15%.

In summary, when the clustering number of the multifractal spectra is six, the explanatory power of the clustering results for all three indicators is maximized. This means that the multifractal structures of the 290 cities have six typical features. The explanatory power of these six typical features for GDP, GDP per capita, and GDP per unit of electricity consumption is 10.51%, 23.51%, and 17.15%, respectively. On average, the explanatory power of the six typical multifractal structures on the energy-economic efficiency is 16.27%.

### *3.3. The Optimized Multifractal Structures of the 290 Cities*

Table 2 shows the results of the risk detector between the multifractal structures and three indicators of energy-economic efficiency (GDP; GDP per capita, named as GDP_POP; and GDP per unit of electricity consumption, named as GDP_EC). As the results show, there is a significant difference (Y) in the mean values of the three indicators among the six typical multifractal structures, which indicates that the six typical multifractal structures have different energy-economic efficiencies. The larger the values of the three indicators are, the higher the energy-economic efficiency of the multifractal structure is. Figure 6 shows the mean values of three energy-economic efficiency indicators for cities with six typical multifractal structures. It can be seen that the mean values of the three indicators within the multifractal structure of class 4 are significantly higher than the other five multifractal structures. Therefore, the multifractal structure of class 4 is the optimized multifractal structure, and the corresponding spectrum is the favorable spectrum. Conversely, although the three energy-economic efficiency indicators of class 5 of the multifractal structure are the lowest, only GDP per capita is significantly different from the other five types of structures, and the mean values of GDP and GDP_EC are not significantly different from the mean values of one or more types of structures, so its spectrum does not have a significant disadvantage and is not considered a harmful spectrum.

**Table 2.** Risk detection for 6 typical multifractal structures.

| **GDP** | **1** | **2** | **3** | **4** | **5** | **6** |
|---|---|---|---|---|---|---|
| 1 | | | | | | |
| 2 | N | | | | | |
| 3 | N | Y | | | | |
| 4 | Y | Y | Y | | | |
| 5 | N | Y | Y | Y | | |
| 6 | N | Y | Y | Y | Y | |
| GDP per capita | 1 | 2 | 3 | 4 | 5 | 6 |
| 1 | | | | | | |
| 2 | N | | | | | |
| 3 | N | Y | | | | |
| 4 | Y | Y | Y | | | |
| 5 | Y | Y | Y | Y | | |
| 6 | N | N | Y | Y | Y | |
| GDP per unit of electricity consumption | 1 | 2 | 3 | 4 | 5 | 6 |
| 1 | | | | | | |
| 2 | N | | | | | |
| 3 | N | Y | | | | |
| 4 | Y | Y | Y | | | |
| 5 | N | Y | Y | Y | | |
| 6 | N | N | Y | Y | Y | |

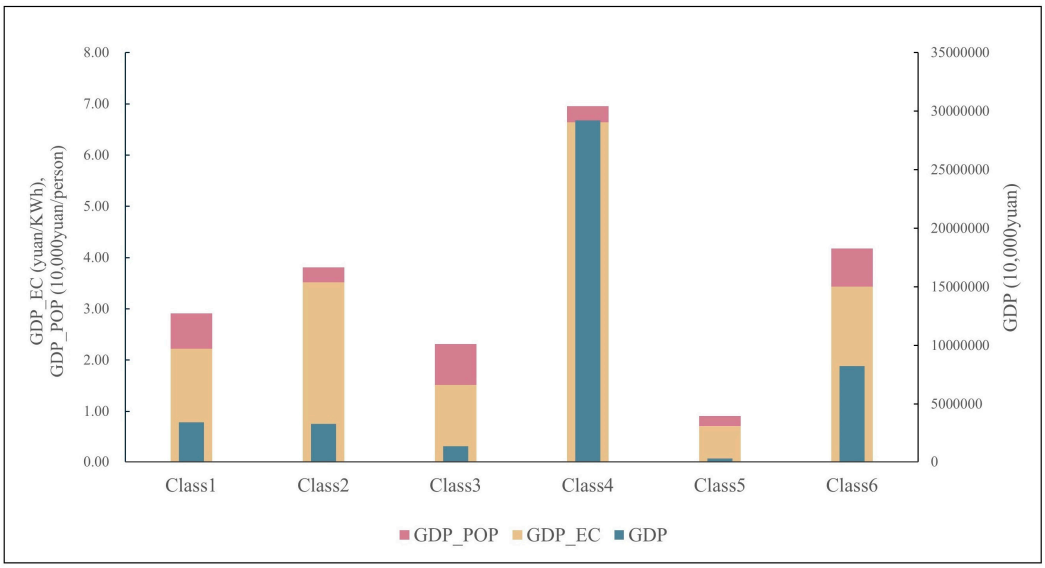


**Figure 6.** Mean values of 3 indicators in the 6 typical multifractal structures.

Figure 7a shows the feature points of the favorable spectrum. Using the interquartile range (IQR) to define outliers, quartiles are points in the dataset that are divided into four equal parts using three segmentation points, known as the first quartile (Q1), second quartile (Q2), and third quartile (Q3). The IQR refers to the distance between Q3 and Q1. If a data point is less than Q1 − 1.5IQR or greater than Q3 + 1.5IQR, then the data point is considered an outlier (blue dots in Figure 7a). The outliers are removed from the feature map, and the retained feature points are shown as orange dots. Figure 7b fits the feature curve of the retained feature points and generates the favorable spectrum. It conforms to a quadratic polynomial equation ($R^2$: 0.78):

$$f = -1.38\alpha^2 + 5.54\alpha - 4.04 \quad (\alpha \in [1.248, 2.104]), \tag{6}$$

where $\alpha$ is the singularity exponent, and f is the fractal dimension. The values of $\alpha$ are within the range of 1.248 and 2.104.

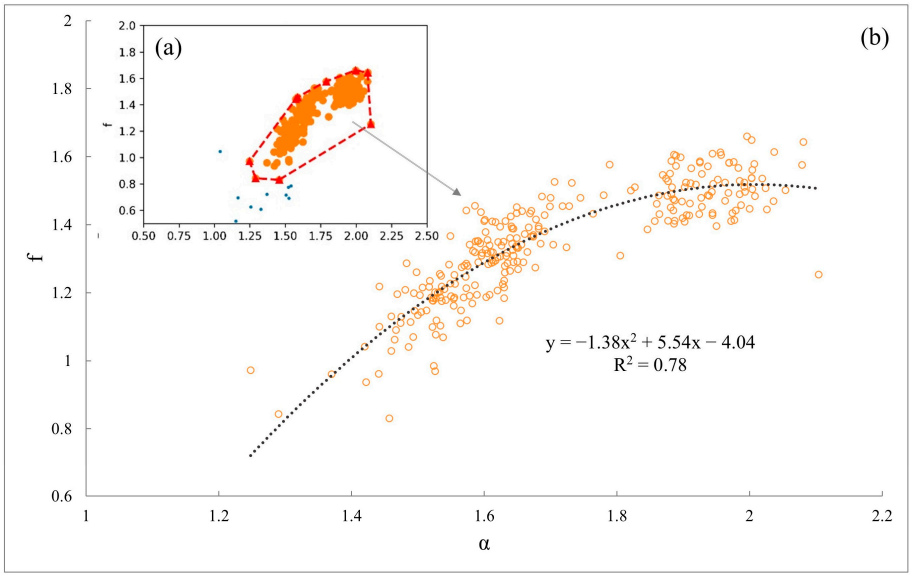


**Figure 7.** The feature points and feature curve of the favorable spectrum. (**a**) The feature points of the favorable spectrum. (**b**) The favorable spectrum generated by fitting the feature points.

In summary, the favorable spectrum curve that was obtained in this study has good energy-economic efficiency. In the context of sustainable urban development and urban renewal, the favorable spectrum provides quantifiable indicators for optimizing urban spatial structures, which can support the intelligent optimization of cities.

### *3.4. Suggestions for Optimizing Urban Multifractal Structures*

Figure 8 shows the multifractal spectrum of six typical urban multifractal structures. The left endpoint of the multifractal spectrum reflects the concentration capacity of high-level central areas and their degree of space-filling. Compared with class 4, high-level central areas in class 2 have a stronger concentration capacity but a weaker degree of space-filling, indicating that resources are over-concentrated in a smaller area and that central areas should be strengthened and expanded.

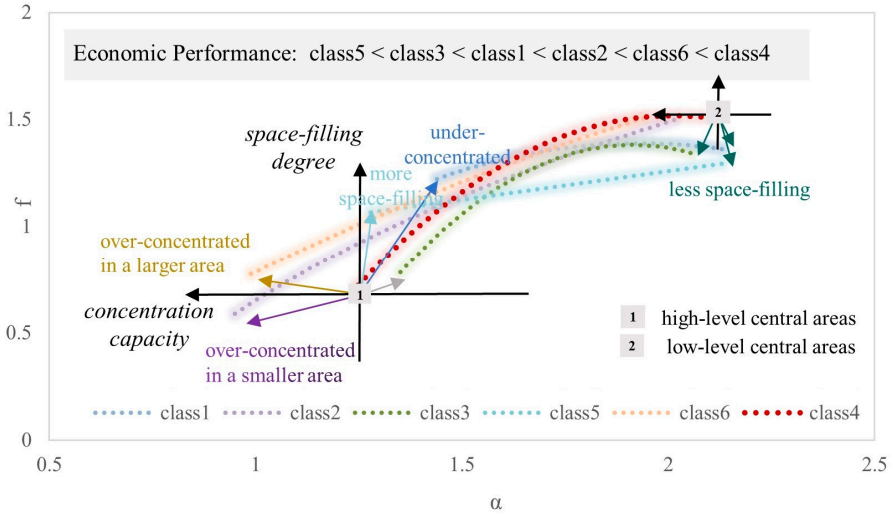


**Figure 8.** Comparison of six typical urban multifractal structures.

Higher-ranking central regions in class 6 have greater concentration capacity and a greater degree of space-filling, indicating that resources are over-concentrated in a larger region and should be radiated to neighboring regions to drive integrated regional development.

The weak concentration capacity and high degree of space-filling in the high-level central areas of class 1 indicate that this type of city lacks a central area that is capable of concentrating resources, that the distribution of resources is relatively scattered, and that the integration of resources should be strengthened, and compact development should be carried out.

The high-ranking central regions of class 5 have a concentration capacity that is close to that of class 4, but with a higher degree of space-filling. Based on the shape of the spectrum of class 5, the difference in the space-filling degree between different central regions is small. The internal hierarchy of the city should be strengthened to create a strong center to drive the development of the city.

The concentration capacity and degree of space-filling of high-level central areas in class 3 are closest to those of class 4, but the space-filling capacity of low-ranking central areas is weaker, indicating that there is sprawl in this class of cities and that the distribution of resources is not centralized, which affects the energy-economic performance of the urban space, and that the development of aggregation in low-ranking central areas should be strengthened to curb the spreading of the cities.

Overall, at the urban scale, the impact of intensive land use on urban energy usage, economic effect, carbon emission, and so on has been widely discussed and recognized [41,42]. This study further analyzes the relationship between the complex spatial structure within

cities and urban energy-economic efficiency. The energy-economic efficiency of urban multifractal structures is affected by the excessive dispersion or excessive concentration of resources. Appropriate dispersion can mitigate the agglomeration of diseconomies due to excessive concentration in a single center [1,43] and can generate higher labor productivity and reduce carbon emissions, thus promoting the development of a green economy [44,45]. Conversely, excessive dispersion can undermine economies of scale and agglomeration effects in urban monocenters [46] and generate greater mobility [47], with a loss of productive efficiency and increased carbon emissions, thus undermining the green economy [45,48]. Therefore, identifying the optimized multifractal structures with higher energy-economic efficiency is of great significance for the development of a green economy.

### *3.5. Limitations and Future Directions*

This study identified optimized multifractal structures by only evaluating the energy-economic performances of the multifractal structures. In the context of the high-quality and sustainable development of towns and cities, a comprehensive performance assessment of the economic, social, and ecological–environmental aspects of urban spatial structure should be carried out [44]. Secondly, as a self-organized complex system, the spatial structure that is formed by cities is in the process of continuous evolution. This study only recognizes urban spatial structures from a temporal cross-section and analyzes the performance of urban spatial structures based on the multifractal perspective through a horizontal comparison between cities. In the future, time series studies can be carried out based on individual cities to longitudinally analyze the law of the evolution of multifractal features of urban spatial structures and changes in their performance and summarize the planning paths for optimal urban development [49,50]. In addition, this study only evaluated the energy-economic performance of the six structures from the perspective of spatial correlation using geodetectors. In the future, spatial causal inference methods such as geographical convergent cross mapping [51] should be drawn on to further analyze the causal relationship between urban multifractal structures and sustainable development.

## 4. Conclusions

A classification-based multifractal method was introduced to identify the spatial structure of 290 Chinese cities. The multifractal structure is a series of scaling exponents, which has the property of scale invariance and solves the scale-dependence problem of the traditional measurement index. For the optimization of urban multifractal structures, the Geodetector method was used iteratively to find the optimized classification with the highest spatial heterogeneity. The main conclusions are as follows:

(1) There are six typical multifractal structures of the 290 Chinese cities. The explanatory power of these six typical multifractal structures for GDP, GDP per capita, and GDP per unit of electricity consumption is 10.51%, 23.51%, and 17.15%, respectively. On average, the explanatory power of the six typical multifractal structures on the energy-economic indicators is 16.27%.

(2) The optimized multifractal structure of cities satisfies the following quadratic polynomial equation: $f = -1.38\alpha^2 + 5.54\alpha - 4.04$ ($\alpha \in [1.248, 2.104]$). The spatial structure performance of a given city can be determined by comparing its multifractal structure with the optimized multifractal structure. The main structural problems included an overly strong or weak concentration capacity of high-level centers, weak hierarchical structures in centers, and the spreading of low-level centers.

In the future, more sustainable development indicators of cities should be used to identify the optimized multifractal structure.

**Author Contributions:** J.W.: Methodology, Formal analysis, and Writing—original draft. B.M.: Resources and Funding acquisition. F.L.: Conceptualization and Supervision. All authors have read and agreed to the published version of the manuscript.

**Funding:** This research was supported by the Academic Research Projects of Beijing Union University (No. ZK30202403, No. ZKZD202305).

**Data Availability Statement:** The original data presented in the study are openly available in Harvard Dataverse at https://doi.org/10.7910/DVN/YGIVCD, Resource and Environment Science and Data Center at https://www.resdc.cn/ (accessed on 25 January 2025), Oak Ridge National Laboratory at https://landscan.ornl.gov/ (accessed on 25 January 2025).

**Conflicts of Interest:** The authors declare no conflicts of interest.

## References

1. Meijers, E.J.; Burger, M.J. Spatial Structure and Productivity in US Metropolitan Areas. *Environ. Plan. A Econ. Space* **2010**, *42*, 1383–1402. [CrossRef]
2. Rao, Y.; Yang, J.; Dai, D.; Wu, K.; He, Q. Urban growth pattern and commuting efficiency: Empirical evidence from 100 Chinese cities. *J. Clean. Prod.* **2021**, *302*, 126994. [CrossRef]
3. Li, W.; Sun, B.; Zhang, T.; Zhang, Z. Panacea, placebo or pathogen? An evaluation of the integrated performance of polycentric urban structures in the Chinese prefectural city-regions. *Cities* **2022**, *125*, 103624. [CrossRef]
4. Sun, B.; Han, S.; Li, W. Effects of the polycentric spatial structures of Chinese city regions on $CO_2$ concentrations. *Transp. Res. Part D Transp. Environ.* **2020**, *82*, 102333. [CrossRef]
5. Han, S.; Sun, B.; Zhang, T. Mono- and polycentric urban spatial structure and $PM_{2.5}$ concentrations: Regarding the dependence on population density. *Habitat Int.* **2020**, *104*, 102257. [CrossRef]
6. She, Q.; Peng, X.; Xu, Q.; Long, L.; Wei, N.; Liu, M.; Jia, W.; Zhou, T.; Han, J.; Xiang, W. Air quality and its response to satellite-derived urban form in the Yangtze River Delta, China. *Ecol. Indic.* **2017**, *75*, 297–306. [CrossRef]
7. Adolphson, M. Estimating a Polycentric Urban Structure. Case Study: Urban Changes in the Stockholm Region 1991–2004. *J. Urban Plan. Dev.* **2009**, *135*, 19–30. [CrossRef]
8. Christaller, W. *Central Places in Southern Germany*; Prentice Hall: Englewood Cliffs, NJ, USA, 1966.
9. Ren, Z.; Jiang, B.; De Rijke, C.; Seipel, S. Characterizing the livingness of geographic space across scales using global nighttime light data. *Int. J. Appl. Earth Obs. Geoinf.* **2024**, *133*, 104136. [CrossRef]
10. Man, X.; Chen, Y. Fractal-Based Modeling and Spatial Analysis of Urban Form and Growth: A Case Study of Shenzhen in China. *ISPRS Int. J. Geo-Inf.* **2020**, *9*, 672. [CrossRef]
11. Murcio, R.; Masucci, A.P.; Arcaute, E.; Batty, M. Multifractal to monofractal evolution of the London street network. *Phys. Rev. E* **2015**, *92*, 062130. [CrossRef]
12. Jiang, B.; De Rijke, C. Structural Beauty: A Structure-Based Computational Approach to Quantifying the Beauty of an Image. *J. Imaging* **2021**, *7*, 78. [CrossRef] [PubMed]
13. Jiang, B.; De Rijke, C. Living Images: A Recursive Approach to Computing the Structural Beauty of Images or the Livingness of Space. *Ann. Am. Assoc. Geogr.* **2023**, *113*, 1329–1347. [CrossRef]
14. Pacheco, P.; Mera, E.; Navarro, G.; Parodi, C. Urban Meteorology, Pollutants, Geomorphology, Fractality, and Anomalous Diffusion. *Fractal Fract.* **2024**, *8*, 204. [CrossRef]
15. Agostinho, F.; Costa, M.; Coscieme, L.; Almeida, C.M.V.B.; Giannetti, B.F. Assessing cities growth-degrowth pulsing by emergy and fractals: A methodological proposal. *Cities* **2021**, *113*, 103162. [CrossRef]
16. Chen, Y.; Zhou, Y. Scaling laws and indications of self-organized criticality in urban systems. *Chaos Solitons Fractals* **2008**, *35*, 85–98. [CrossRef]
17. Jiang, B.; Wei, H.; Feng, Y. Controversies Concerning Emergency Tracheal Intubation in Patients with COVID-19. *J. Anesth. Transl. Med.* **2023**, *2*, 15–18. [CrossRef]
18. Lu, C.; Liu, Y. Effects of China's urban form on urban air quality. *Urban Stud.* **2016**, *53*, 2607–2623. [CrossRef]
19. Zhang, H.; Li, Z. Fractality and Self-Similarity in the Structure of Road Networks. *Ann. Assoc. Am. Geogr.* **2012**, *102*, 350–365. [CrossRef]
20. Guo, S.; Pei, T.; Xie, S.; Song, C.; Chen, J.; Liu, Y.; Shu, H.; Wang, X.; Yin, L. Fractal dimension of job-housing flows: A comparison between Beijing and Shenzhen. *Cities* **2021**, *112*, 103120. [CrossRef]
21. Jiang, B. Head/tail breaks for visualization of city structure and dynamics. *Cities* **2015**, *43*, 69–77. [CrossRef]
22. Jiang, B.; Yin, J. Ht-Index for Quantifying the Fractal or Scaling Structure of Geographic Features. *Ann. Assoc. Am. Geogr.* **2014**, *104*, 530–540. [CrossRef]

23. Long, Y.; Chen, Y. Multifractal scaling analyses of urban street network structure: The cases of twelve megacities in China. *PLoS ONE* **2021**, *16*, e0246925. [CrossRef]
24. Salat, H.; Murcio, R.; Yano, K.; Arcaute, E. Uncovering inequality through multifractality of land prices: 1912 and contemporary Kyoto. *PLoS ONE* **2018**, *13*, e0196737. [CrossRef] [PubMed]
25. Sémécurbe, F.; Tannier, C.; Roux, S.G. Spatial Distribution of Human Population in France: Exploring the Modifiable Areal Unit Problem Using Multifractal Analysis. *Geogr. Anal.* **2016**, *48*, 292–313. [CrossRef]
26. Tan, X.; Huang, B.; Batty, M.; Li, J. Urban Spatial Organization, Multifractals, and Evolutionary Patterns in Large Cities. *Ann. Am. Assoc. Geogr.* **2021**, *111*, 1539–1558. [CrossRef]
27. Wang, J.; Lu, F.; Liu, S. A classification-based multifractal analysis method for identifying urban multifractal structures considering geographic mapping. *Comput. Environ. Urban Syst.* **2023**, *101*, 101952. [CrossRef]
28. Lu, Y.; Tang, J. Fractal Dimension of a Transportation Network and its Relationship with Urban Growth: A Study of the Dallas-Fort Worth Area. *Environ. Plan. B Plan. Des.* **2004**, *31*, 895–911. [CrossRef]
29. Lan, T.; Li, Z.; Zhang, H. Urban Allometric Scaling Beneath Structural Fractality of Road Networks. *Ann. Am. Assoc. Geogr.* **2019**, *109*, 943–957. [CrossRef]
30. Lan, T.; Peng, Q.; Wang, H.; Gong, X.; Li, J.; Shi, Z. Exploring Allometric Scaling Relations between Fractal Dimensions of Metro Networks and Economic, Environmental and Social Indicators: A Case Study of 26 Cities in China. *ISPRS Int. J. Geo-Inf.* **2021**, *10*, 429. [CrossRef]
31. Xu, Q.; Dong, Y.; Yang, R. Influence of different geographical factors on carbon sink functions in the Pearl River Delta. *Sci. Rep.* **2017**, *7*, 110. [CrossRef]
32. Cao, W.; Dong, L.; Wu, L.; Liu, Y. Quantifying urban areas with multi-source data based on percolation theory. *Remote Sens. Environ.* **2020**, *241*, 111730. [CrossRef]
33. Liu, S.; Shen, J.; Liu, G.; Wu, Y.; Shi, K. Exploring the effect of urban spatial development pattern on carbon dioxide emissions in China: A socioeconomic density distribution approach based on remotely sensed nighttime light data. *Comput. Environ. Urban Syst.* **2022**, *96*, 101847. [CrossRef]
34. Li, Y.; Liu, X. How did urban polycentricity and dispersion affect economic productivity? A case study of 306 Chinese cities. *Landsc. Urban Plan.* **2018**, *173*, 51–59. [CrossRef]
35. Wang, J.; Lu, F. Modeling the electricity consumption by combining land use types and landscape patterns with nighttime light imagery. *Energy* **2021**, *234*, 121305. [CrossRef]
36. Chen, Z.; Yu, B.; Yang, C.; Zhou, Y.; Yao, S.; Qian, X.; Wang, C.; Wu, B.; Wu, J. An extended time series (2000–2018) of global NPP-VIIRS-like nighttime light data from a cross-sensor calibration. *Earth Syst. Sci. Data* **2021**, *13*, 889–906. [CrossRef]
37. Xu, X. China GDP Spatial Distribution Kilometer Grid Dataset, Resource and Environmental Science Data Registration and Publishing System. 2017. Available online: http://www.resdc.cn/DOI (accessed on 25 January 2025).
38. Rose, A.; McKee, J.; Sims, K.; Bright, E.; Reith, A.; Urban, M. LandScan Global 2019 [Data Set]. Oak Ridge National Laboratory, 2020. Available online: https://landscan.ornl.gov/ (accessed on 25 January 2025).
39. Wang, J.; Li, X.; Christakos, G.; Liao, Y.; Zhang, T.; Gu, X.; Zheng, X. Geographical Detectors-Based Health Risk Assessment and its Application in the Neural Tube Defects Study of the Heshun Region, China. *Int. J. Geogr. Inf. Sci.* **2010**, *24*, 107–127. [CrossRef]
40. Nassar, Y.F.; Alsadi, S.Y.; El-Khozondar, H.J.; Ismail, M.S.; Al-Maghalseh, M.; Khatib, T.; Sa'ed, J.A.; Mushtaha, M.H.; Djerafi, T. Design of an isolated renewable hybrid energy system: A case study. *Mater. Renew. Sustain. Energy* **2022**, *11*, 225–240. [CrossRef]
41. He, P.; Wang, Q.-C.; Shen, G.Q. The Carbon Emission Implications of Intensive Urban Land Use in Emerging Regions: Insights from Chinese Cities. *Urban Sci.* **2024**, *8*, 75. [CrossRef]
42. Wang, Y.; Niu, Y.; Li, M.; Yu, Q.; Chen, W. Spatial structure and carbon emission of urban agglomerations: Spatiotemporal characteristics and driving forces. *Sustain. Cities Soc.* **2022**, *78*, 103600. [CrossRef]
43. Lin, D.; Allan, A.; Cui, J. The impact of polycentric urban development on commuting behaviour in urban China: Evidence from four sub-centres of Beijing. *Habitat Int.* **2015**, *50*, 195–205. [CrossRef]
44. Zhang, T.; Sun, B.; Li, W. The economic performance of urban structure: From the perspective of Polycentricity and Monocentricity. *Cities* **2017**, *68*, 18–24. [CrossRef]
45. Wang, Y.; Sun, B.; Zhang, T. Do polycentric urban regions promote functional spillovers and economic performance? Evidence from China. *Reg. Stud.* **2022**, *56*, 63–74. [CrossRef]
46. Melo, P.C.; Graham, D.J.; Levinson, D.; Aarabi, S. Agglomeration, accessibility and productivity: Evidence for large metropolitan areas in the US. *Urban Stud.* **2017**, *54*, 179–195. [CrossRef]
47. Parr, J.B. Cities and Regions: Problems and Potentials. *Environ. Plan. A Econ. Space* **2008**, *40*, 3009–3026. [CrossRef]
48. Li, W.; Sun, B.; Zhao, J.; Zhang, T. Economic performance of spatial structure in Chinese prefecture regions: Evidence from night-time satellite imagery. *Habitat Int.* **2018**, *76*, 29–39. [CrossRef]
49. Chen, Y. Fractal dimension evolution and spatial replacement dynamics of urban growth. *Chaos Solitons Fractals* **2012**, *45*, 115–124. [CrossRef]

50. Chen, Y.; Huang, L. Modeling growth curve of fractal dimension of urban form of Beijing. *Phys. A Stat. Mech. Its Appl.* **2019**, *523*, 1038–1056. [CrossRef]
51. Gao, B.; Yang, J.; Chen, Z.; Sugihara, G.; Li, M.; Stein, A.; Kwan, M.-P.; Wang, J. Causal inference from cross-sectional earth system data with geographical convergent cross mapping. *Nat. Commun.* **2023**, *14*, 5875. [CrossRef]